

Interpolation for Image deformation in PIV

Byoung Jae Kim¹, Chetan Swarup¹ & Hyung Jin Sung¹

¹Department of Mechanical Engineering, Korea Advanced Institute of Science and Technology, Korea

Keywords: PIV, Image deformation, interpolation, Bias and Random Errors

Abstract: Several interpolations for image deformation in PIV were evaluated. A synthetic image program was developed for this evaluation. The tested interpolation methods are bilinear, quadratic, truncated sinc, windowed sinc, cubic, Lagrange, Gaussian 2nd and 6th interpolators. The bias and random errors were evaluated for uniform displacement in the range of 0~3.0 pixels using the synthetic images. We also measured the time cost of each interpolator with respect to kernel size. The cubic interpolator with 6×6 kernel showed the best results in terms of the performance and time cost.

1. Introduction

PIV (particle image velocimetry) has been a main tool to measure instantaneous velocity distribution using cross-correlation of two consecutive particle images. The conventional cross-correlation has many limitations in strong-velocity-gradient flows because of the fixed location and size of two interrogation windows. To overcome this, many advanced techniques in image processing have been developed.

Huang et al (1993) proposed PID (particle image distortion), according to flow patterns, to improve the limitations in the conventional cross-correlation where the velocity gradient is high. The process started with a conventional cross-correlation. The resultant velocity distribution was then used to shift and deform the interrogation windows to compensate for particle-pair loss due to in-plane motion. Scarano (2000) applied the multi-grid technique that reduces the window size successively in accordance with previous result to PID. Tokumaru and Dimotakis (1995) gave a general approach to the problem of matching from fluid motion. They proposed to enlarge the dimensionality of the optimization domain introducing the spatial derivatives of displacement distribution as independent parameters. Scarano (2004) added the multi-grid approach to the correlation using the 2nd derivatives.

Above techniques are based on the processing of continuous images, which are obtained by interpolating digital images. In PIV, because the interpolation for pixel intensity at a sub-pixel location is ahead of non-linear image processing to extract a velocity vector, the PIV performance could depend greatly on what kind of interpolation is adopted. Huang et al (1993) adopted the linear interpolation for PID and 0.25 pixel uncertainty was showed. Tokumaru and Dimotakis (1995) also used the same interpolation for the 2nd order of the series expansion process in experiments. Instead, Scarano (2000, 2002, 2004) selected the truncated sinc

interpolation for window deformation, which is more complicate. Fincham and Delerce (2000) used the 2D-spline and indicated the weak reflection of true distribution beneath the scale of 1 pixel.

Since the deformation of the second interrogation window in time is described as a continuous 2D plane, we must know the pixel intensity at a sub-pixel location in the deformed window, which is realized through a kind of interpolation. An interpolator has been however intuitively selected for realizing continuous image, without quantitative effects on the interpolation performance. Therefore, the objective of this study is to quantitatively evaluate and compare the performances and the time cost of frequently used interpolators. The tested PIV algorithm is the 1st order deformation proposed by Huang et al (1993), since the PIV techniques mentioned earlier are similar or succeed to it. A synthetic image program is developed for the present evaluation. In this paper, the bias and random errors in the uniform displacement are dealt with for each interpolator with different kernel sizes (2×2 to 10×10).

2. Window deformation

2.1. Cross-correlation matching

Many PIV techniques employ an optimization that relies on some form of a cross-correlation function,

$$\max_a \int_A f_1(x)f_2(x+a)dx^2, \quad (1)$$

where \mathbf{a} is the displacement vector to be determined by the procedure and A is the correlation domain. The intensity distribution of the image $f(x)$ is known at times t_1 and t_2 , i.e., $f_1(x)$ and $f_2(x)$. The 1st order approximation of the displacement in the neighborhood of \mathbf{x}_0 is expressed through a Taylor series truncated at the linear term,

$$\mathbf{a} = \mathbf{a}(x) = \mathbf{a}(x_0) + (\nabla \mathbf{a})_0(x - x_0). \quad (2)$$

The conventional cross-correlation analysis can be referred to as the zero-order matching approximation. Instead, Eq.1 with Eq.2 is referred to as the 1st order approximation (Fig.1). The main purpose of this operation is to achieve matching between regions where the continuum deformation is accounted for, in terms of translation, rotation, shearing and dilation.

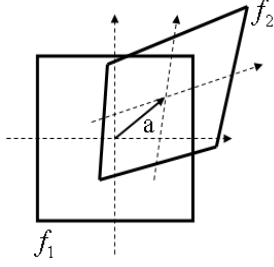


Figure 1. Window transformation of the particle image

2.2. Interpolation

Deformation process needs image re-sampling in order to obtain particle intensity information at sub-pixel locations in f_2 image. Interpolation for the re-sampling can be described formally as the convolution of the discrete image samples $f(m, n)$ with the continuous 2D impulse response ${}_{2D}h(x, y)$ of a 2D reconstruction filter (Lehmann et al 1999).

$$f(x, y) = \sum_m \sum_n f(m, n) \cdot {}_{2D}h(m - x, n - y), \quad (3)$$

where $f(x, y)$ represents the image intensity retrieved at a sub-pixel location. Usually, symmetrical and separable interpolation kernels are used to reduce the computation complexity.

$${}_{2D}h(x, y) = h(x)h(y). \quad (4)$$

Following the sampling theory, the original image $f(x, y)$ can be reconstructed perfectly from its samples $f(m, n)$ using

$${}^{ideal}h(x) = \frac{\sin(\pi x)}{\pi x} = \text{sinc}(x). \quad (5)$$

Some fundamental properties of any interpolator can be derived from this ideal interpolation function.

$$\begin{cases} h(0) = 1 \\ h(x) = 0, |x| = 1, 2, \dots \end{cases} \quad (6)$$

The kernels satisfying Eq.6 are called interpolators. Particularly, the sum of all samples should be one for any displacement $0 \leq d < 1$,

$$\sum_{m=-\infty}^{\infty} h(d + m) = 1. \quad (7)$$

This means that the mean brightness of the image is not affected if the image is interpolated (DC-constant).

$$\sum_{m=-\infty}^{\infty} h(d + m) = 1 \Leftrightarrow \begin{cases} H(0) = 1 \\ H(f) = 0, |f| = 1, 2, \dots \end{cases} \quad (8)$$

The conditions in Eq.8 are not sufficient but necessary in the context of interpolation, but they are used to distinguish DC-constant from DC-inconstant. Below are some $h(x)$ with kernel size N .

- Truncated sinc interpolator

$${}^{tsinc}h_N = \begin{cases} {}^{ideal}h(x), & 0 \leq |x| < N/2 \\ 0, & \text{elsewhere} \end{cases} \quad (9)$$

- Sinc interpolator windowed by Blackman-Harris window

$${}^{wsinc}h_N = \begin{cases} {}^{ideal}h(x) \cdot w(x), & 0 \leq |x| < N/2 \\ 0, & \text{elsewhere} \end{cases} \quad (10)$$

$$w(x) = 0.42323 + 0.49755 \cos(2\pi x / N) + 0.07922 \cos(4\pi x / N)$$

- Linear interpolator

$${}^{linear}h = \begin{cases} 1 - |x|, & 0 \leq |x| < 1 \\ 0, & \text{elsewhere} \end{cases} \quad (11)$$

- Quadratic interpolator ($a = 1$)

$${}^{quad}h = \begin{cases} -2a|x|^2 + \frac{a+1}{2}, & 0 \leq |x| < \frac{1}{2} \\ a|x|^2 - \frac{2a+1}{2}|x| + \frac{3(a+1)}{4}, & \frac{1}{2} \leq |x| < \frac{3}{2} \\ 0, & \text{elsewhere} \end{cases} \quad (12)$$

- Cubic interpolator ($a = -0.5$)

$${}^{cubic}h_2 = \begin{cases} 2|x|^3 - |x|^2 + 1, & 0 \leq |x| < 1 \\ 0, & \text{elsewhere} \end{cases} \quad (13)$$

$${}^{cubic}h_4 = \begin{cases} (a+2)|x|^3 - (a+3)|x|^2 + 1, & 0 \leq |x| < 1 \\ a|x|^3 - 5a|x|^2 + 8a|x| - 4a, & 1 \leq |x| < 2 \\ 0, & \text{elsewhere} \end{cases} \quad (14)$$

$${}^{cubic}h_6 = \begin{cases} \frac{6}{5}|x|^3 - \frac{11}{5}|x|^2 + 1, & 0 \leq |x| < 1 \\ -\frac{3}{5}|x|^3 + \frac{16}{5}|x|^2 - \frac{27}{5}|x| + \frac{14}{5}, & 1 \leq |x| < 2 \\ \frac{1}{5}|x|^3 - \frac{8}{5}|x|^2 + \frac{21}{5}|x| - \frac{18}{5}, & 2 \leq |x| < 3 \\ 0, & \text{elsewhere} \end{cases} \quad (15)$$

$${}^{cubic}h_8 = \begin{cases} \frac{67}{56}|x|^3 - \frac{123}{56}|x|^2 + 1, & 0 \leq |x| < 1 \\ -\frac{33}{56}|x|^3 + \frac{177}{56}|x|^2 - \frac{75}{14}|x| + \frac{39}{14}, & 1 \leq |x| < 2 \\ \frac{9}{56}|x|^3 - \frac{75}{56}|x|^2 + \frac{51}{14}|x| - \frac{45}{14}, & 2 \leq |x| < 3 \\ -\frac{3}{56}|x|^3 + \frac{33}{56}|x|^2 - \frac{15}{14}|x| + \frac{18}{14}, & 3 \leq |x| < 4 \\ 0, & \text{elsewhere} \end{cases} \quad (16)$$

•Lagrange interpolator

$$Lagrange h_N = \begin{cases} \prod_{j=0, j-N/2+1 \neq n}^{N-1} \frac{n-i-x}{n-i}, & n-1 \leq x < n \quad (17) \\ 0, & \text{elsewhere} \end{cases}$$

$$i = j - N/2 + 1, \quad n: \text{integer}$$

•2nd order Gaussian interpolator

$$G h_N = \begin{cases} G^0(x, 2\gamma_2) - \gamma_2 G^2(x, \gamma_2), & 0 \leq |x| < N/2 \quad (18) \\ 0, & \text{elsewhere} \end{cases}$$

$$G^0(x, \beta) = \frac{1}{\sqrt{2\pi\beta}} e^{-x^2/2\beta},$$

$$\gamma_2 = \frac{1}{2\pi} \left(\frac{1}{\sqrt{2}} + 1 \right) \approx 0.4638115$$

•6th order Gaussian interpolator (19)

$$G h_N = \begin{cases} G^0(x, 2\gamma_6) - \gamma_6 G^2(x, \gamma_6) - \frac{\gamma_6^3}{24} G^6(x, \gamma_6), & 0 \leq |x| < N/2 \\ 0, & \text{elsewhere} \end{cases}$$

$$\gamma_6 = \frac{1}{2\pi} \left(\frac{1}{\sqrt{2}} + 1 + \frac{15}{24} \right) \approx 0.8655995$$

3. Results and discussion

3.1. Artificial image generation

The intensity distribution of a particle was modeled as a Gaussian profile. The maximum value of the Gaussian profile was then given according to the particle location inside the laser sheet in the out-of-plane direction (Okamoto et al 2000). In this study, particles with $\bar{d}_p = 2$ pixels and $\sigma_p = 1$ pixel were randomly generated onto 8 bit gray images. The number of particles was about 14500 inside the volume of $512 \times 512 \times 7$ (pixel³). Each pixel value was obtained by integrating the Gaussian intensity profile over the pixel.

3.2. Uniform displacement

As a peak-estimator, Gaussian fitting was used, and the vector validation and the replacement of error vectors were not performed. The interrogation window size was set 32×32 .

Figures 2 and 3 show the bias errors of the 1st order deformation with the windowed sinc and cubic interpolators, respectively, as a function of uniform displacement (0~3.0 pixels).

The bias errors tend to decrease at every multiple of 0.5 pixel, showing a sinusoidal shape. This is well known as a peak-locking phenomenon, which is elucidated by Fincham and Spedding (1997). One interesting observation that can be concluded from Figs. 2 and 3 is that there exists an optimal kernel size. We can see that the performance curves converge from about 6×6 kernel size. Similar patterns are found in the

other interpolators. Moreover, interpolators satisfying Eqs.6~8 more show the good performances. For example, the bias error of the Gaussian 6th interpolation is better than that of the Gaussian 2nd interpolation. In Lagrange interpolation, there is no clear convergence in the performance with regard to the kernel size.

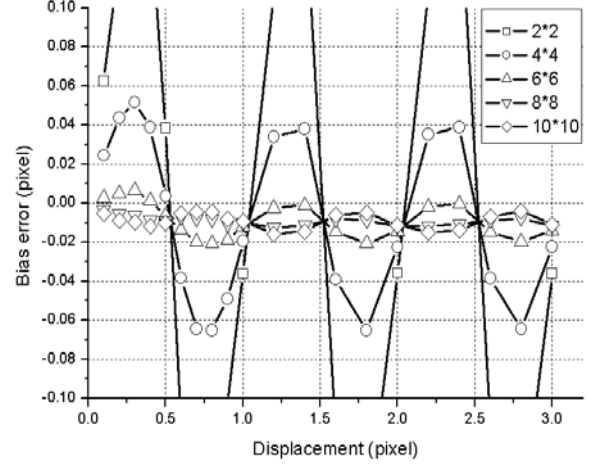


Figure 2. Windowed truncated sinc interpolation

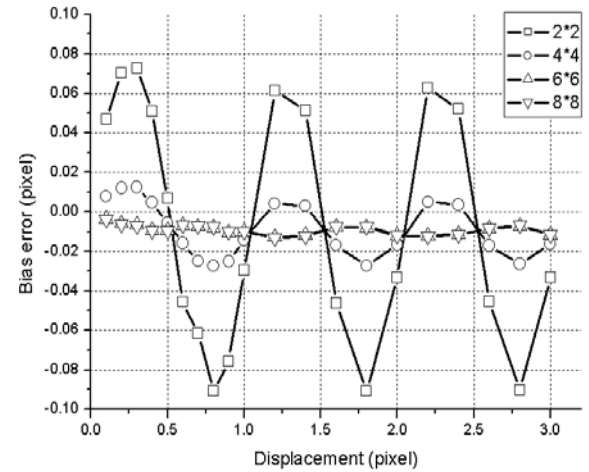


Figure 3. Cubic interpolation

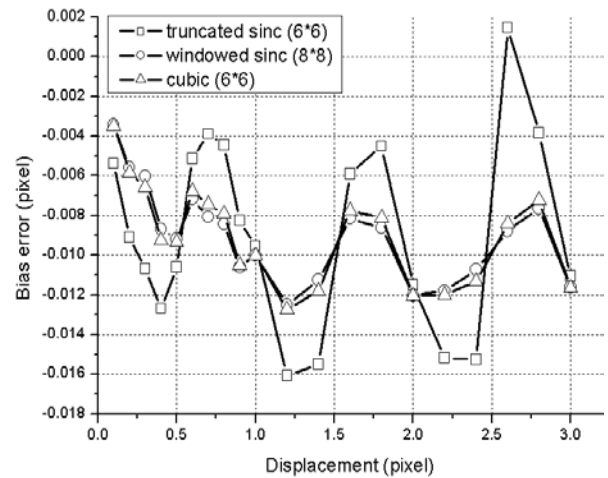


Figure 4. Comparison of the interpolation with the best kernel size

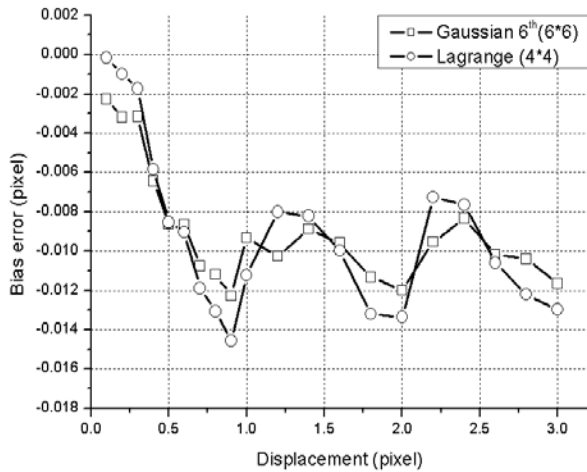


Figure 5. Bias errors of each interpolator with the best kernel size

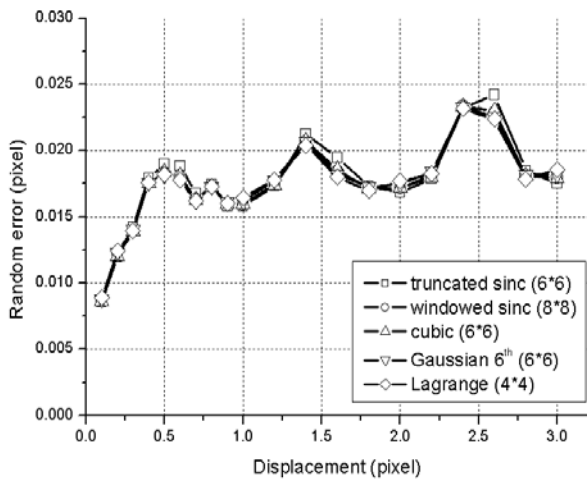


Figure 2. Random errors of each interpolator with the best kernel size

Table 1. Comparison of the bias errors of interpolators Figs.4~5 (uniform displacement)

	N	mean (pixel)	standard deviation (pixel)
tsinc	6×6	-0.00904	0.00481
wsinc	8×8	-0.00917	0.00237
cubic	6×6	-0.00916	0.00248
Gaussian 6 th	6×6	-0.00907	0.00296
Lagrange	4×4	-0.00922	0.00423

Table 2. Time cost with respect to kernel size for some interpolators (unit: second)

	2×2	4×4	6×6	8×8	10×10
linear	4				
tsinc	5	10	17	25	38
wsinc	8	18	34	60	91
Cubic	5	8	14	23	
Gaussian 6 th	13	40	81	150	226
Lagrange	4	11	26	49	80

Figures 4 and 5 compare graphically the bias errors of different interpolators. Here, each performance line is taken from each interpolation with the best kernel size. The mean value and standard deviation of each

performance line in Figs.4~5 are tabulated in Table. 1. We can see very small difference in the mean value, but there is big difference in the standard deviation. From these results, the windowed sinc and cubic interpolators give stable error performance for uniform flows. In addition to the error performance, the time cost of each interpolation for 1024×1024 pixel² were measured and given in Table 2. It is shown that the interpolators having kinds of polynomials work faster. From these, it can be concluded in uniform flow that the cubic interpolator with kernel size 6×6 is optimal terms of the error performance and time cost.

4. Future plan and conclusions

The bias and random errors of interpolations for the 1st order image deformation in PIV were investigated. The results show that the cubic interpolation with 6×6 kernel size is the most effective scheme in uniform displacement. In the range of 0~3.0 pixel uniform displacement, the bias error was less than about -0.015 pixel and the random error was about 0.02 pixel. To examine the effects of interpolators more, we are going to test them in linear shear and sinusoidal motions.

References

Fincham, A.M. & Delerce, G. 2000 Advanced optimization of correlation image velocimetry algorithms. *Experiments in Fluids*, Suppl, pp. 13

Fincham, A.M. & Spedding, G.R. 1997 Low cost, high resolution DPIV for measurement of turbulent fluid flow. *Experiments in Fluids*, Vol. 23, pp. 23

Huang, H.T., Fiedler, H.E. & Wang, J.J. 1993 Limitation and improvement of PIV. *Experiments in Fluids*, Vol. 15, pp. 168

Lehmann, T.M., Gonner, C. & Spitzer, K. 1999 Survey: Interpolation methods in medical image processing. *IEEE Transaction on Medical Imaging*, Vol. 18, No. 11, pp. 1049

Okamoto, K., Nishio, S., Saga, T. & Kobayasi, T. 2000 Standard images for particle-image-velocimetry. *Measurement Science & Technology*, Vol. 11, pp. 685

Scarano, F. 2004 A super-resolution particle image velocimetry interrogation approach by means of velocity second derivatives correlation. *Measurement Science & Technology*, Vol. 15, pp. 475

Scarano, F. 2002 Iterative image deformation methods in PIV. *Measurement Science & Technology*, Vol. 13, R1

Scarano, F. & Riethmuller, M.L. 2000 Advances in iterative multi-grid in PIV image processing. *Experiments in Fluids*, Suppl, pp. 51

Tokumaru, P.T. & Dimotakis, P.E. 1995 Image-correlation velocimetry. *Experiments in Fluids*, Vol. 19, pp. 1